Journal of Catalysis 314 (2014) 142–148

Contents lists available at ScienceDirect

Journal of Catalysis

journal homepage: www.elsevier.com/locate/jcat

Supported iron nanoparticles for the hydrodeoxygenation of microalgal oil to green diesel

Kapil Kandel [a,b], James W. Anderegg [a], Nicholas C. Nelson [a,b], Umesh Chaudhary [a,b], Igor I. Slowing [a,b,*]

[a] U.S. Department of Energy, Ames Laboratory, Ames, IA 50011-3020, USA
[b] Department of Chemistry, Iowa State University, Ames, IA 50011-3111, USA

ARTICLE INFO

Article history:
Received 11 November 2013
Revised 4 April 2014
Accepted 9 April 2014

Keywords:
Mesoporous silica nanoparticles
Iron nanoparticles
Fatty acids
Hydrodeoxygenation
Microalgae oil
Green diesel

ABSTRACT

Iron nanoparticles supported on mesoporous silica nanoparticles (Fe-MSN) catalyze the hydrotreatment of fatty acids with high selectivity for hydrodeoxygenation over decarbonylation and hydrocracking. The catalysis is likely to involve a reverse Mars–Van Krevelen mechanism, in which the surface of iron is partially oxidized by the carboxylic groups of the substrate during the reaction. The strength of the metal–oxygen bonds that are formed affects the residence time of the reactants facilitating the successive conversion of carboxyl first into carbonyl and then into alcohol intermediates, thus dictating the selectivity of the process. The selectivity is also affected by the pretreatment of Fe-MSN, the more reduced the catalyst the higher the yield of hydrodeoxygenation product. Fe-MSN catalyzes the conversion of crude microalgal oil into diesel-range hydrocarbons.

1. Introduction

The increasing energy demand and concerns over the gradual depletion of fossil fuels have attracted significant amount of research to the exploration of alternative energy sources [1,2]. In this context, microalgae are considered as one of the most promising renewable energy resources owing to their short harvest cycle, small cultivation area, high lipid content (up to 80% of their dry weight), and minimum greenhouse gas emission [3,4].

The major components of microalgal oil are free fatty acids (FFAs) and triglycerides. These can be converted to fatty acid methyl esters (FAMEs) by catalytic reaction with methanol and used as biodiesel. However, due to the degree of unsaturation and high oxygen content of the FAMEs, issues such as poor storage stability, marginal cold flow, and engine compatibility limit their widespread use [5,6]. An alternate technology to produce biofuels from microalgal oil is through hydrotreating with Ni, Co, and Mo sulfides or noble metal catalysts such as Pd and Pt supported on metal oxides [7–14]. While the high price of the noble metals can be avoided by using the sulfided catalysts, slow desulfurization reduces their activity and contaminates the fuel [7,9,15]. Furthermore, these catalysts have shown poor selectivity, favoring cracking and decarbonylation over hydrodeoxygenation to produce broad hydrocarbon distributions [16]. In an effort to establish a more economical sulfur-free catalyst to upgrade renewable oils, Lercher has demonstrated the hydrodeoxygenation of microalgae oil to alkanes by cascade reactions on bifunctional catalysts based on Ni and an acidic zeolite [14,17]. Following work by the same group illustrated the selectivity toward decarbonylation route by supporting Ni catalyst on ZrO_2 which directed the conversion through two parallel pathways [18].

The success of Ni in the conversion of renewable feedstocks into green diesel [14,19,28] stimulates the exploration of other inexpensive transition metals as catalysts for the process. Considering its rich redox-chemistry, high natural abundance and low price, iron emerges as an appealing candidate for this kind of conversion. While many researchers have been studying iron catalysts in the Fischer–Tropsch synthesis for several decades [20,21], the activity and selectivity of these species for the hydrodeoxygenation of fatty acids has not been much explored. To contribute to the efforts for economical and efficient catalysts for upgrading renewable feedstocks to green diesel, we report the synthesis of iron nanoparticles supported on mesoporous silica nanomaterials (Fe-MSN), and their application in the hydrotreatment of fatty acids and crude microalgal oil.

2. Experimental

2.1. Materials

Pluronic P104 (>99.8%) was generously provided by BASF. Tetramethyl orthosilicate (TMOS, 98%), oleic acid (⩾99.0%) and

* Corresponding author at: 2756 Gilman Hall, Iowa State University, Ames, IA 50011-3111, USA. Fax: +1 515 294 4709.
E-mail address: islowing@iastate.edu (I.I. Slowing).

http://dx.doi.org/10.1016/j.jcat.2014.04.009
0021-9517/

Sylon (N,O-bis(trimethylsilyl)trifluoroacetamide, 99.3% and trimethylchlorosilane, 99.3%, 99:1) were purchased from Sigma Aldrich. Iron (III) Nitrate [$Fe(NO_3)_3{\cdot}9H_2O$] (100%), hydrochloric acid (37.3%, ACS certified) and hexanes (certified, mixture of isomers, boiling range 1.0 °C) were purchased from Fisher Scientific. All reagents were used as received without further purification.

2.2. Catalyst preparation

MSN was prepared using a nonionic block co-polymer Pluronic P104 surfactant [22]. In a typical synthesis, P104 (7.0 g) was dissolved in aqueous HCl (273.0 g, 1.6 M). After stirring for 1 h at 56 °C, tetramethylorthosilicate (TMOS, 10.64 g) was added and stirred for additional 24 h. The resulting mixture was further hydrothermally treated for 24 h at 150 °C in a high-pressure reactor. Upon cooling to room temperature, the white solid was collected by filtration, washed with copious amounts of methanol, and dried in air. To remove the surfactant P104, the MSN material was heated at a ramp rate of 1.5 °C min^{-1} and maintained at 550 °C for 6 h. MSN was then mixed with water and stirred at room temperature in order to rehydrate and regenerate the silanol groups, followed by filtration and drying. For impregnation, $Fe(NO_3)_3{\cdot}9H_2O$ (0.40 mmol, 0.16 g) was completely dissolved in water (0.48 mL). To this solution, the rehydrated MSN (0.4 g) was added and mixed. The solid mixture was calcined in air at a heating rate of 10 °C min^{-1} to 300 °C and maintained at that temperature for 3 h followed by reduction at 400 °C for 6 h in a constant flow of H_2 (1.67 mL s^{-1}).

2.3. Characterization

Surface analysis of the catalyst was performed by nitrogen sorption isotherms at −196 °C in a Micromeritics Tristar analyzer. The surface areas were calculated by the Brunauer–Emmett–Teller (BET) method, and the pore size distribution was calculated by the Barrett–Joyner–Halenda (BJH) method. Pretreatment of samples for surface area measurement was done by flowing N_2 for 6 h at 100 °C. Powder X-ray diffraction patterns were obtained with a Rigaku Ultima IV diffractometer using Cu target at 40 kV and 44 mA, and samples were analyzed in the 0.8–90 $2\theta^\circ$ at a scan rate of 1 $2\theta^\circ$ min^{-1}. Cu Kβ was removed using a monochromator. Crystallite size was estimated from modeling the diffraction at 44.6 $2\theta^\circ$ with OriginPro software and incorporating the FWHM into the Scherrer equation ($d = K\lambda/\beta\cos\theta$, where d is the estimated crystallite size, K is the shape factor, λ is the wavelength of the Cu Kα, β is the line broadening at half the maximum intensity in radians, and θ is the Bragg angle) [27]. For transmission electron microscopy measurements, an aliquot of the powder was sonicated in methanol for 15 min. A single drop of this suspension was placed on a lacey carbon-coated copper TEM grid and dried in air. The TEM examination was completed on a Tecnai G2 F20 electron microscope operated at 200 kV. Average particle size was calculated using ImageJ software based on five representative TEM images (100 particles). Fourier transform infrared (FT-IR) spectra were recorded on Nicolet Nexus 470. Samples were diluted with KBr (about 5 wt%) and made into pellets for analysis in transmission mode. To measure the Fe loading, samples (2.0 mg) were digested for 20 h in aqueous HF and HCl solution (0.18% and 5% respectively) and analyzed in a Perkin Elmer Optima 2100 DV ICP-OES. Temperature-programmed reduction was performed in a Micromeritics AutoChem II using a flow of H_2 in Argon (10.13%, 50 mL min^{-1}) ramping from 40 °C to 500 °C at a rate of 10 °C min^{-1}. XPS analysis was done with a PHI 5500 multi-technique system using a standard Al X-ray source. Since the samples were mounted on two-sided scotch tape, charge correction was accomplished by shifting the spectra so that silicon 2p peak was at 103.3 eV.

2.4. Catalytic activity measurements

All catalytic reactions were performed in a 100-mL batch reactor (Parr Instruments). In a typical experiment, the catalyst (10 mg) and oleic acid solution in hexanes (1 mM, 10 mL) were added in the reactor. The reactor was purged three times with H_2 and was then pressurized with H_2 to 30 bar at ambient temperature. For kinetics study, the reaction was carried out at 290 °C for 1, 2, 3, 4, 5, and 6 h with constant stir rate (500 rpm). The reaction was allowed to cool to room temperature and the catalyst was separated. The reaction product was mixed with 1 mL Sylon (N,O-bis(trimethylsilyl)trifluoroacetamide and trimethylchlorosilane, 99:1) and heated to 70 °C for 2 h for further derivatization. The final mixture was analyzed in an Agilent GC–MS (7890A, 5975C) with a HP – 5MS column. Runs started at 100 °C for 5 min, then ramped to 200 °C at a rate of 20 °C min^{-1} held for 25 min, and then ramped to 280 °C at 20 °C min^{-1} holding for 5 min at this temperature. Methyl nonadecanoate was used as an internal standard. Conversion was defined as mole% and calculated as moles of converted oleic acid per mole of starting oleic acid times 100%. Yields were defined as mole% and were calculated as moles of each product per mole of starting oleic acid times 100%.

Similar experiment was conducted on crude microalgal oil obtained from Solix Biofuels, Inc. by adding Fe-MSN catalyst (10 mg) to a solution of microalgal oil (10 mg in 10 mL hexanes) and heating to 290 °C under 30 bar H_2 for 6 h.

3. Results and discussion

3.1. Synthesis of Fe-MSN

The textural properties of MSN support and Fe-MSN catalyst are summarized in Table 1. ICP measurement indicated that 6.0 wt% Fe was immobilized on the MSN. Formation of the Fe nanoparticles led to approximately 10% decrease in the surface area and pore volume of the support; however, its nitrogen sorption isotherm remained type IV confirming retention of the mesoporous character (Fig. 1a) [23]. TEM and STEM imaging suggested that the Fe nanoparticles were located mainly inside the pores of MSN (Fig. 1b). Low-angle XRD analysis confirmed that the structure of the support was not affected by the formation of Fe nanoparticles, as it preserved the *p6mm* pattern characteristic of SBA-15 type materials (Fig. 1c) [24]. Wide-angle XRD showed a pattern of peaks corresponding to the body-centered cubic phase of crystalline iron nanoparticles (JCPDS card No. 89-7194, Fig. 1d) [25,26]. The wide reflections indicated small crystallite size of the iron nanoparticles. Estimation using Scherrer equation indicated that their size (9.9 nm) was similar to the width of the mesopores (10.9 nm), suggesting nanoparticle growth was restricted by pore width [27]. This observation was supported by estimation of the average size of the Fe nanoparticles from TEM images (10.7 nm), which was only slightly smaller than the pore width (Fig. S1).

Table 1
Textural properties of the support and catalyst.

Material	Surface area (m^2 g^{-1})	Pore volume (cm^3 g^{-1})	Pore diameter (nm)
MSN	331	0.97	11.1
Fe-MSN	295	0.88	10.9

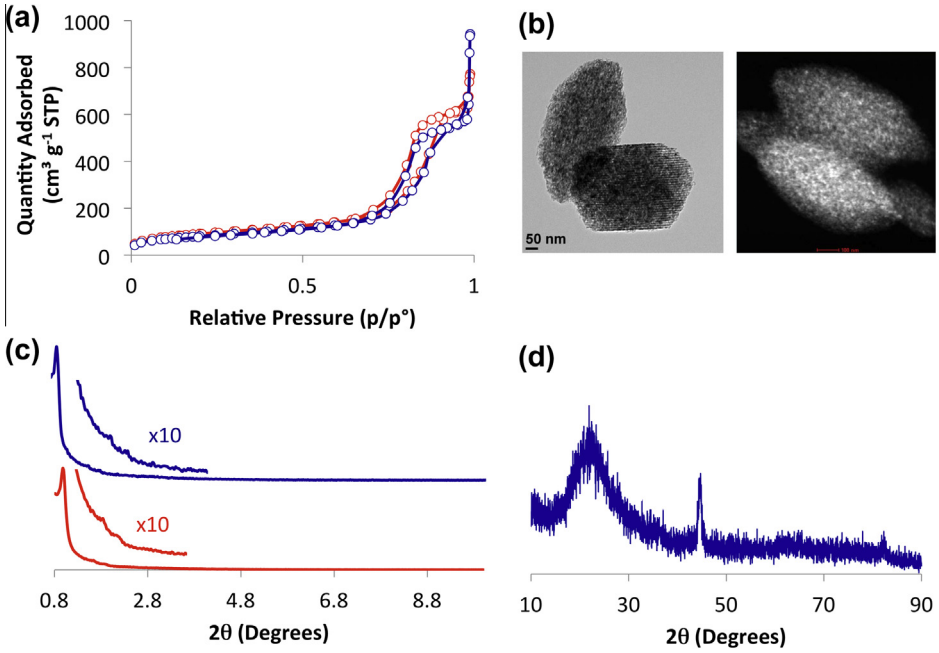

Fig. 1. (a) N_2 sorption isotherms of MSN (red) and Fe-MSN (blue), (b) TEM (left) and HAADF-STEM (right) images of Fe-MSN, (c) XRD patterns of MSN (red) and Fe-MSN (blue), insets show 10× magnified 110 and 200 reflections, and (d) wide-angle XRD of Fe-MSN. (For interpretation of the references to color in this figure legend, the reader is referred to the web version of this article.)

3.2. Oleic acid hydrotreatment with Fe-MSN

The kinetics of hydrotreatment of oleic acid (1 mM, 10 mL) with Fe-MSN (10 mg) at 290 °C and 30 bar H_2 pressure is shown in Fig. 2. No oleic acid was detected after 0.5 h and the major hydrocarbon product obtained after 6 h was *n*-octadecane, indicating hydrodeoxygenation was the major reaction route. The yield of *n*-octadecane (C_{18}) increased continuously to 83% at 6 h, while that of *n*-heptadecane (C_{17}) grew slowly to 12% after 6 h (Fig. 2a). In sharp contrast to the hydrogenation of oleic acid using nickel supported on MSN under the same reaction conditions (72% hydrocracking, 25% C_{17} and 3% C_{18}) [28], the hydrocracking was almost eliminated with Fe-MSN catalyst as it was only observed after 6 h reaction (3% yield).

Stearic acid and 1-octadecanol were observed with highest yields at early reaction times, peaking before 0.5 and 2 h respectively and then decreasing, which suggested that both species are reaction intermediates (Fig. 2b). Since stearic acid disappeared earlier than octadecanol, it is likely that the reaction proceeded initially by a fast hydrogenation of C=C, followed by reduction of the COOH group to alcohol, which eventually underwent hydrodeoxygenation to give the major reaction product. The yield of *n*-octadecane increased linearly with the decrease in 1-octadecanol until 5 h, supporting the notion that the alcohol is an intermediate in the hydrodeoxygenation pathway (Fig. S2).

The formation of *n*-octadecane from 1-octadecanol could take place as a two-step process, first involving dehydration of 1-octadecanol to give 1-octadecene, which would then be hydrogenated to the saturated product (Scheme 1, pathway a). *n*-Heptadecane could form either by direct decarboxylation of stearic acid or by decarbonylation of octadecanal, which could also be an intermediate in the formation of 1-octadecanol (Scheme 1, pathway b). The quick conversion of oleic acid to stearic acid suggests that the hydrogenation of double bonds must be very fast under the reaction conditions. Recent reports show that suspensions of iron nanoparticles catalyze alkene hydrogenation at room temperature and pressures as low as 1 bar H_2 [29]. Therefore, if octadecene and heptadecene form as intermediates, they should be transformed at a high rate into octadecane and heptadecane, respectively. Indeed, performing the Fe-MSN-catalyzed hydrogenation of oleic acid under milder conditions allowed the detection of both alkenes (about 2% yields at 10 bar H_2 and 270 °C).

The Fe-catalyzed reduction of acetic acid to acetaldehyde takes place at 1 bar H_2 in the range of 250–350 °C [30–32]. This suggests

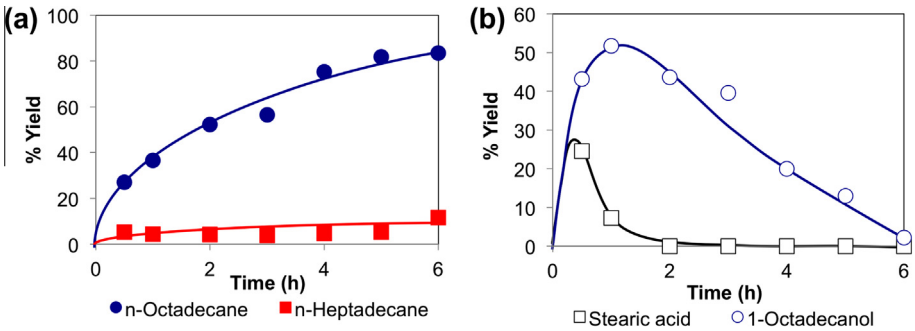

Fig. 2. Kinetics of oleic acid hydrotreatment catalyzed by Fe-MSN: (a) hydrocarbon products, and (b) reaction intermediates.

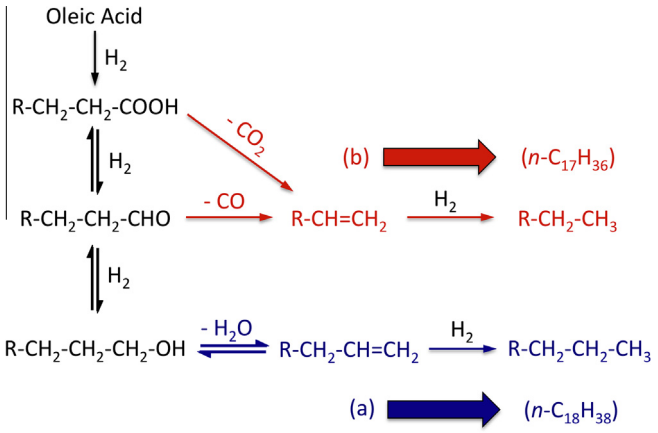

Scheme 1. Possible mechanisms for the conversion of oleic acid into *n*-octadecane (blue, a) and *n*-heptadecane (red, b) from the intermediates 1-octadecanol and octadecanal, respectively. R = *n*-pentadecyl. (For interpretation of the references to color in this figure legend, the reader is referred to the web version of this article.)

that Fe-MSN should be able to catalyze the hydrogenation of stearic acid to octadecanal under the conditions employed in this work. Yet, the equilibrium constant for the hydrogenation of octadecanal to 1-octadecanol at 260 °C is approximately 57, which explains why the aldehyde is scarce under our reaction conditions [18]. Octadecanal could only be observed when performing the reaction at a lower temperature (2.4% yield after 6 h at 30 bar H_2 and 230 °C). Because aldehyde was not detected at 250 °C or higher reaction temperatures, the aldehyde reduction rate to the alcohol was concluded to be fast over Fe-MSN under the reaction condition employed. Thus, if under our reaction conditions the rate of interconversion between the aldehyde and alcohol is fast, the ratio of *n*-heptadecane to *n*-octadecane products in the overall reaction must be controlled by the relative rates of aldehyde decarbonylation and alcohol dehydration. Fe-MSN may favor the latter reaction, for iron-based catalysts promote the dehydration of ethanol at temperatures above 200 °C [33].

The production of liquid hydrocarbons was very low at 230 °C but increased dramatically with temperature to almost 100% at 290 °C (Fig. 3a). Analysis of hydrocarbon distribution (Fig. 3b and c) revealed that the increase of yield in this range was mainly due to *n*-octadecane (from under 1% at 230 °C to 83% at 290 °C). The yield of *n*-hepadecane also increased with temperature, but to a smaller extent (from under 1% at 230 °C to 16% at 310 °C). The products of hydrocracking were not observed at 230 °C but were detected only at temperatures higher than 250 °C, with an increase from 1% at 250 °C to 7% at 310 °C. It must be noted that while the yields of both decarbonylation and hydrocracking products kept increasing from 290 °C to 310 °C, the yield of *n*-octadecane dropped from 83% at 290 °C to 72% at 310 °C. This suggests that temperatures higher than 290 °C tend to favor decarbonylation and hydrocracking at the expense of hydrodeoxygenation. These observations suggest that the apparent activation energies for the processes leading to decarbonylation and hydrocracking should be higher than the apparent activation energies of the steps that lead to hydrodeoxygenation when Fe-MSN is used as a catalyst.

As expected, the conversion of oleic acid was proportional to the pressure of hydrogen applied (Fig. 4a). However, at 270 °C, the total hydrocarbon yield showed little sensitivity to an increase in pressure from 10 to 20 bar, going only from 33% to 36% and requiring higher pressures to approach to full conversion. Consistent with previous reports, low hydrogen pressures increased the selectivity for decarbonylation and hydrocracking, whereas high hydrogen pressures favored heavily hydrodeoxygenation (Fig. 4b)

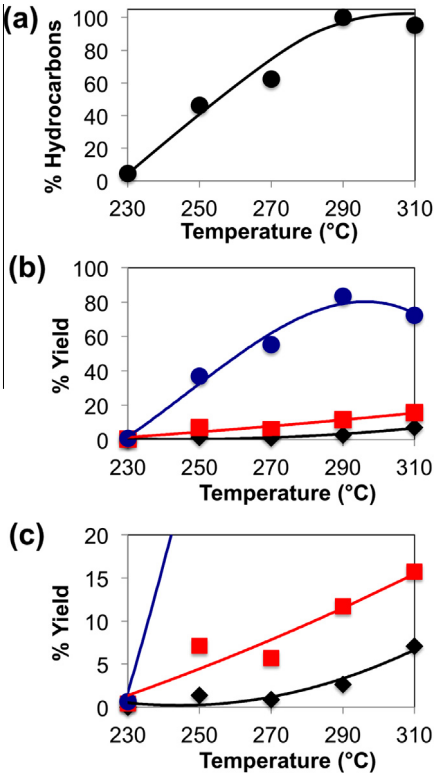

Fig. 3. Effect of temperature on (a) the yield and (b) distribution of hydrocarbons in the Fe-MSN-catalyzed hydrotreatment of oleic acid (6 h yields, 30 bar H_2). (c) Same plot as (b) showing details in the scale 0–20%. Blue circles correspond to *n*-octadecane, red squares to *n*-heptadecane and black rhombi to hydrocracking products. (For interpretation of the references to color in this figure legend, the reader is referred to the web version of this article.)

[2,18]. This dependence of selectivity on hydrogen pressure is likely the result of the participation of H_2 in the equilibrium between octadecanal and 1-octadecanol, the branching step in the process. As hydrogen is required to convert the octadecanal into 1-octadecanol, increasing the amount of the gas shifts the equilibrium toward the alcohol favoring the route to *n*-octadecane, while decreasing the amount of the gas has the opposite effect leading to the *n*-heptadecane pathway.

3.3. Mechanism of oleic acid hydrotreatment with Fe-MSN

As mentioned above, iron oxides have been reported as catalysts for the selective reduction of carboxylic acids to aldehydes [34]. Pestman and co-workers demonstrated that the reduction of acetic acid to acetaldehyde over iron oxides required the formation of a Fe(0) phase on the surface of the oxide [31]. They proposed that hydrogen was first bound at the metallic sites and then spilled over to reduce the acid, which was bound at defect sites in the oxide [32,35,36]. Kinetic studies by Rachmady and Vannice supported this mechanism as they demonstrated that the reaction fits a Langmuir–Hinshelwood model for two reactants binding at two different types of site [30,37]. XRD analysis of our catalyst showed only metallic iron and gave no evidence of the oxide (Fig. 1d). However, given its redox potential, Fe can be readily oxidized by mere exposure to air, forming sub-nanometer layers of oxide in less than 1 min [38,39]. Indeed, XPS analysis revealed the presence of iron oxide in the catalyst (Fig. S3). Thus, the absence of iron oxide peaks in the XRD was likely due to low concentration and/or lack of crystallinity. Interestingly, the spent catalyst showed a less-defined XRD pattern, in which the Fe(0)

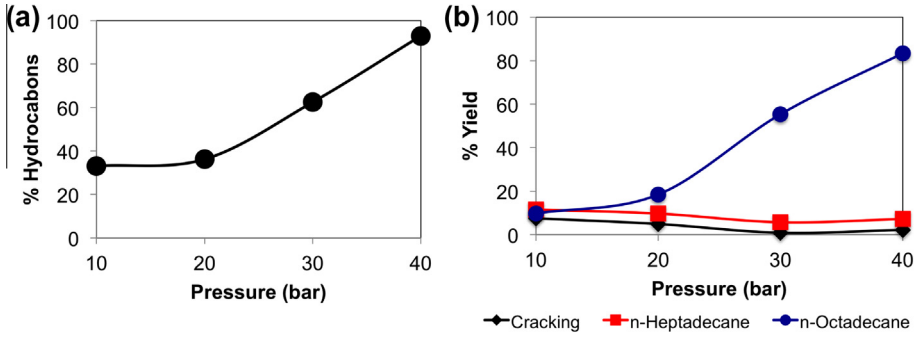

Fig. 4. Effect of H_2 pressure on (a) the yield and (b) distribution of hydrocarbons in the Fe-MSN-catalyzed hydrotreatment of oleic acid at 270 °C (6 h yields). In (b) blue circles correspond to *n*-octadecane, red squares to *n*-heptadecane and black rhombi to hydrocracking products. (For interpretation of the references to color in this figure legend, the reader is referred to the web version of this article.)

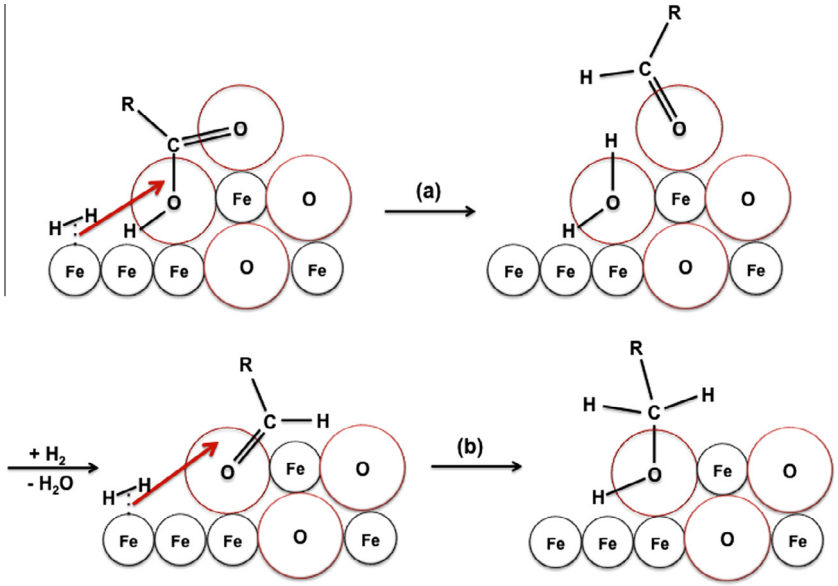

Scheme 2. Proposed mechanism of the hydrogenation of carboxylic groups on the surface of the partially oxidized Fe nanoparticles of Fe-MSN: (a) reduction to aldehyde, and (b) further reduction to alcohol. The oxygen atoms eliminated from the FFA may either escape as water or become part of a growing iron oxide lattice.

peak almost disappeared and a weak reflection at 35°, possibly belonging to the oxide, emerged (Fig. S4). These observations suggested that the process involved an active transformation of the surface of the catalyst as it was continuously reduced by the H_2 and oxidized by the carboxylic acid, through a reverse Mars–Van Krevelen mechanism. In contrast to the work by Pestman et al., our original catalyst was Fe(0) rather than iron oxides, and the reaction was performed at much higher H_2 pressure. These differences had important consequences, as starting with Fe(0) provided more surface for H_2 to bind, which along with the higher H_2 concentration prevented the reaction from stopping at the carbonyl stage (Scheme 2). Consistently with the proposed reaction pathways, if the reduction stopped at the carbonyl stage, the main product of hydrogenation under our reaction conditions should have been *n*-heptadecane (decarbonylation). Conversely, if the reduction continued to form the alcohol, the main product would have been *n*-octadecane (hydrodeoxygenation), which indeed was the case with Fe-MSN.

To evaluate if the degree of oxidation of iron controlled whether the reaction stopped at the carbonyl or the alcohol stage, we compared the selectivities of hydrotreatment of oleic acid using iron-MSN materials reduced with H_2 at increasing temperatures. The temperature-programmed reduction (TPR) profile of the parent material (iron nitrate-impregnated MSN after calcination in air) indicated two reduction steps with T_m at 240 °C and 345 °C (Fig. S5), suggesting the transition between different oxidized states of iron-MSN and the conversion into the final Fe(0)-MSN, respectively. XRD analyses of the original calcined iron oxide-MSN and of samples reduced at 240 °C and 350 °C gave no reflections, suggesting lack of crystallinity of the iron species. However, XPS analyses of the same samples confirmed the presence of oxidized iron in them (Fig. S6). Consistent with the hypothetical mechanism, the C_{18}:C_{17} selectivities of the hydrotreatment of oleic acid using the non-reduced material and the samples reduced at 240 °C, 350 °C, 400 °C and 500 °C were proportional to the temperature of reduction of iron in the catalysts (Fig. 5). The non-reduced material gave the lowest yield of *n*-octadecane, suggesting that a significant fraction of oleic acid stopped at the carbonyl stage leading the way to the decarbonylation product *n*-heptadecane. To the contrary, the reduced materials led to higher selectivities for *n*-octadecane, which results from the formation of 1-octadecanol. This behavior is also consistent with the observed changes in hydrocarbon selectivity with time (decrease for *n*-octadecane and increase for *n*-heptadecane), as the Fe-MSN catalyst gradually

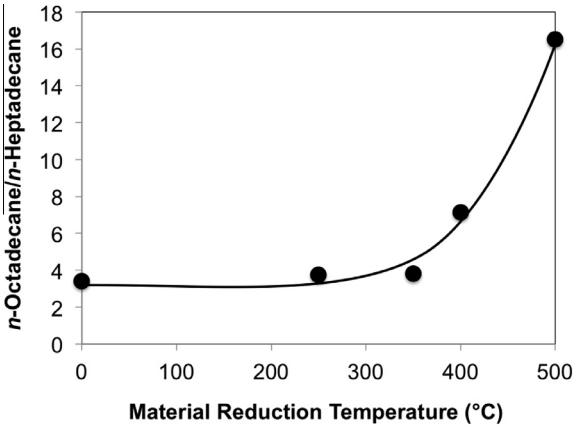

Fig. 5. Product selectivity as a function of the oxidation state of the catalyst.

Table 2
Fatty acid composition of microalgal oil.[a]

C_{12}[b]	C_{14}	$C_{16:2}$	$C_{16:1}$	C_{16}	$C_{18:3}$	$C_{18:2}$	C_{18}	$C_{20:5}$
0.32	4.59	1.13	21.88	22.34	3.94	14.79	0.67	30.32

[a] Crude microalgal oil from Solix Biofuels, Inc.
[b] First subindexes correspond to number of carbon atoms, subindexes following colons correspond to the number of unsaturations in the chains.

changed from Fe(0) to a mixture of the metallic phase and an oxide (Figs. 2a and S1).

It is likely that the tendency of Fe to favor hydrodeoxygenation over decarbonylation in the hydrotreatment of oleic acid is directly related to the strength of the Fe–O bonds that form during the reaction. The strength of metal–oxygen bonds can be estimated from the heats of formation of the highest oxides of the metal [35]. For instance, Fe forms stronger metal–oxygen bonds than Ni, which favors decarbonylation over hydrodeoxygenation when supported on silica [18,28]. Thus, the capacity to form stronger bonds allows for longer retention times of the oxygenated intermediates, which prevents the reaction from stopping at the carbonyl stage and lead to higher hydrodeoxygenation yields.

3.4. Conversion of microalgae oil into green diesel

A crude microalgal oil extract (Solix Biofuel, Inc., 10 mg in 10 mL hexanes) was directly hydrotreated with 10 mg of Fe-MSN at 290 °C under 30 bar H_2 in batch mode. GC–MS analysis showed that the fatty acid composition of the extract consisted mainly of unsaturated C_{16}, C_{18} and C_{20} fatty acids (72.1 mol%) and saturated C_{14} and C_{16} fatty acids (27 mol%, Table 2). Hydrotreatment of the crude oil for 6 h using Fe-MSN as a catalyst gave 67% conversion, the products being 16% alcohols, 33% unsaturated hydrocarbons and 18% saturated hydrocarbons (Figs. 6 and S6). All of the remaining 33% FFAs were saturated, even if most of the acids in the original extract were unsaturated (72.1%). This behavior is consistent with our observation that the hydrogenation of double bonds was the first step in the hydrotreatment of oleic acid. The high ratio of C_{18}:C_{17} products (6.4:1) obtained during the hydrotreatment of microalgal extract is very similar to the ratio we obtained during the hydrotreatment of oleic acid (6.9:1), which is also consistent with our observation that Fe-MSN favors hydrodeoxygenation over decarbonylation.

Only a fraction of the fatty acids in microalgal oil exist as free acids, while another part occur as di- or triglycerides. Thus, the reduction of the fatty acid glycerides to hydrocarbons requires an initial hydrogenolysis step. This additional step implies a higher hydrogen consumption, which consequently should affect product yield and distribution [40]. The presence of octadecene after hydrotreatment of the crude microalgae oil is consistent with the observation of unsaturated hydrocarbons at low H_2 pressure (Fig. 4), as the availability of H_2 is diminished by its consumption in the hydrodeoxygenation and hydrogenolyses. Further studies to elucidate the detailed kinetics and mechanism on hydrotreatment of triglycerides with Fe-MSN and pathways to decrease the hydrogen consumption are currently under investigation in our laboratory.

4. Conclusions

Supported iron nanoparticles are efficient and sulfur-free alternative catalysts for converting microalgal oil into green diesel. Fe-MSN catalyzes the hydrogenation of oleic acid to stearic acid, which is further reduced to aldehyde and alcohol intermediates. The H_2 pressure of the reaction controls the equilibrium between aldehyde and alcohol intermediates directing it to two main pathways: either decarbonylation of the aldehyde or dehydration of the alcohol. Both of these processes give unsaturated hydrocarbons, which get further hydrogenated to give liquid alkanes. The process that involves dehydration of the alcohol has a lower temperature barrier than that of decarbonylation and hydrocracking when Fe-MSN is used as a catalyst and is the major pathway at 290 °C and 30 bar H_2. This pathway gives full hydrodeoxygenation of oleic acid with the highest carbon economy. Fe-MSN catalyzes this reaction by dynamically changing its surface composition through a reverse

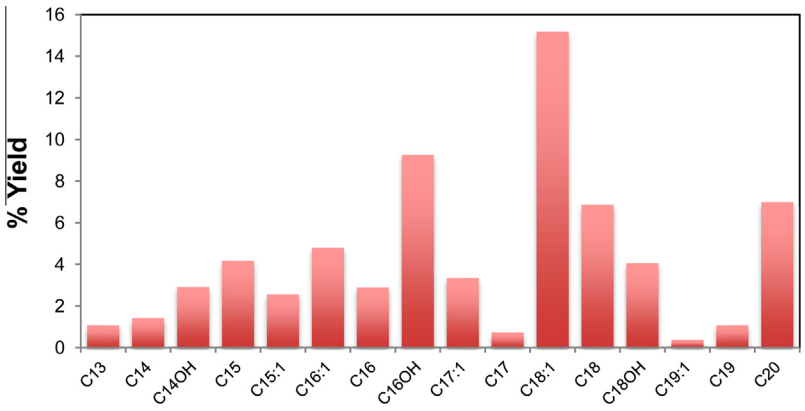

Fig. 6. Distribution of liquid products of Fe-MSN-catalyzed hydrotreatment of crude microalgal oil extract (Solix biofuels, Inc.; 6 h 290 °C and 30 bar H_2). First subindexes correspond to number of carbon atoms, subindexes following colons correspond to the number of unsaturations in the chains, OH designates alcohol.

Mars–Van Krevelen mechanism in which carboxylic acids oxidize the metallic surface and react with spilled-over hydrogen. It is likely that the high selectivity of Fe-MSN for hydrodeoxygenation results from the strength of the Fe–O bond, which allows for residence times that are long enough to complete the reduction of substrate and intermediates. Tuning the degree of oxidation of Fe in the catalyst allows controlling the ratio of hydrodeoxygenation to decarbonylation of the hydrocarbon products. Using Fe-MSN as a catalyst in the hydrotreatment of crude microalgal extract leads to diesel-range hydrocarbons. In addition to the hydrodeoxygenation of the FFAs, Fe-MSN catalyzed the hydrogenolysis of glycerides. Further investigation of the mechanism and conditions of Fe-MSN-catalyzed hydrogenolysis of glycerides are ongoing in our laboratory. We envision that additional understanding of the various conversions involved in the hydrotreatment of complex oils will lead to the creation of more inexpensive and efficient catalysts for converting biorenewable feedstocks into liquid hydrocarbon fuels.

Acknowledgments

This research was supported at the Ames Laboratory by the U.S. Department of Energy, Office of Basic Energy Sciences. Ames Laboratory is operated for the U.S. Department of Energy by Iowa State University under Contract No. DE-AC02-07CH11358.

Appendix A. Supplementary material

Supplementary data associated with this article can be found, in the online version, at http://dx.doi.org/10.1016/j.jcat.2014.04.009.

References

[1] R. Xing, A.V. Subrahmanyam, H. Olcay, W. Qi, G.P. van Walsum, H. Pendse, G.W. Huber, Green Chem. 12 (2010) 1933.
[2] S. Lestari, P. Mäki-Arvela, J. Beltramini, G.Q.M. Lu, D.Y. Murzin, ChemSusChem 2 (2009) 1109.
[3] E. Molina Grima, E.H. Belarbi, F.G. Acién Fernández, A. Robles Medina, Y. Chisti, Biotechnol. Adv. 20 (2003) 491.
[4] Y.C. Sharma, B. Singh, J. Korstad, Green Chem. 13 (2011) 2993.
[5] P. Šimáček, D. Kubička, G. Šebor, M. Pospíšil, Fuel 88 (2009) 456.
[6] P. Priecel, D. Kubička, L. Čapek, Z. Bastl, P. Ryšánek, Appl. Catal. A 397 (2011) 127.
[7] G.W. Huber, P. O'Connor, A. Corma, Appl. Catal. A 329 (2007) 120.
[8] D. Kubička, L. Kaluža, Appl. Catal. A 372 (2010) 199.
[9] D. Kubička, J. Horáček, Appl. Catal. A 394 (2011) 9.
[10] M. Snåre, I. Kubičková, P. Mäki-Arvela, K. Eränen, J. Wärnå, D.Y. Murzin, Chem. Eng. J. 134 (2007) 29.
[11] S. Lestari, P.i. Mäki-Arvela, H. Bernas, O. Simakova, R. Sjöholm, J. Beltramini, G.Q.M. Lu, J. Myllyoja, I. Simakova, D.Y. Murzin, Energy Fuels 23 (2009) 3842.
[12] B. Rozmysłowicz, P. Mäki-Arvela, S. Lestari, O. Simakova, K. Eränen, I. Simakova, D. Murzin, T. Salmi, Top. Catal. 53 (2010) 1274.
[13] P. Do, M. Chiappero, L. Lobban, D. Resasco, Catal. Lett. 130 (2009) 9.
[14] C. Zhao, T. Bruck, J.A. Lercher, Green Chem. 15 (2013) 1720.
[15] T.R. Viljava, R.S. Komulainen, A.O.I. Krause, Catal. Today 60 (2000) 83.
[16] Y. Yang, C. Ochoa-Hernández, V.A. de la Peña O'Shea, J.M. Coronado, D.P. Serrano, ACS Catal. 2 (2012) 592.
[17] B. Peng, Y. Yao, C. Zhao, J.A. Lercher, Angew. Chem. Int. Ed. 51 (2012) 2072.
[18] B. Peng, X. Yuan, C. Zhao, J.A. Lercher, J. Am. Chem. Soc. 134 (2012) 9400.
[19] W. Song, C. Zhao, J.A. Lercher, Chem. Eur. J. 19 (2013) 9833.
[20] G.P. Van Der Laan, A.A.C.M. Beenackers, Catal. Rev. 41 (1999) 255.
[21] D.L. Huber, Small 1 (2005) 482.
[22] T.-W. Kim, I.I. Slowing, P.-W. Chung, V.S.-Y. Lin, ACS Nano 5 (2010) 360.
[23] Y. Wan, D.Y. Zhao, Chem. Rev. 107 (2007) 2821.
[24] D. Zhao, J. Feng, Q. Huo, N. Melosh, G.H. Fredrickson, B.F. Chmelka, G.D. Stucky, Science 279 (1998) 548.
[25] S. Peng, C. Wang, J. Xie, S. Sun, J. Am. Chem. Soc. 128 (2006) 10676.
[26] L.M. Lacroix, N. Frey Huls, D. Ho, X. Sun, K. Cheng, S. Sun, Nano Lett. 11 (2011) 1641.
[27] H. Borchert, E.V. Shevchenko, A. Robert, I. Mekis, A. Kornowski, G. Grübel, H. Weller, Langmuir 21 (2005) 1931.
[28] K. Kandel, C. Frederickson, E.A. Smith, Y.-J. Lee, I.I. Slowing, ACS Catal. 3 (2013) 2750.
[29] P.-H. Phua, L. Lefort, J.A.F. Boogers, M. Tristany, J.G. de Vries, Chem. Commun. (2009) 3747.
[30] W. Rachmady, M.A. Vannice, J. Catal. 208 (2002) 158.
[31] E.J. Grootendorst, R. Pestman, R.M. Koster, V. Ponec, J. Catal. 148 (1994) 261.
[32] R. Pestman, R.M. Koster, E. Boellaard, A.M. van der Kraan, V. Ponec, J. Catal. 174 (1998) 142.
[33] T. Zaki, J. Colloid Interface Sci. 284 (2005) 606.
[34] J.C. Kuriacose, S.S. Jewur, J. Catal. 50 (1977) 330.
[35] R. Pestman, R.M. Koster, J.A.Z. Pieterse, V. Ponec, J. Catal. 168 (1997) 255.
[36] C. Doornkamp, V. Ponec, J. Mol. Catal. A 162 (2000) 19.
[37] W. Rachmady, M.A. Vannice, J. Catal. 208 (2002) 170.
[38] A. Cabot, V.F. Puntes, E. Shevchenko, Y. Yin, L. Balcells, M.A. Marcus, S.M. Hughes, A.P. Alivisatos, J. Am. Chem. Soc. 129 (2007) 10358.
[39] Y.-P. Sun, X.-Q. Li, J. Cao, W.-X. Zhang, H.P. Wang, Adv. Colloid Interface Sci. 120 (2006) 47.
[40] B. Donnis, R. Egeberg, P. Blom, K. Knudsen, Top. Catal. 52 (2009) 229.